Miscibility and Crystallization Behaviors of Poly(3-hydroxybutyrate-*co*-11%-4-hydroxybutyrate)/ Poly(3-hydroxybutyrate-*co*-33%-4-hydroxybutyrate) Blends

Zhiyuan Lan,[1] Jueyu Pan,[1] Xiaojuan Wang,[1] Jianyun He,[2] Kaitian Xu[1]

[1]*Multidisciplinary Research Center, Shantou University, Shantou, Guangdong 515063, China*
[2]*College of Materials Science and Engineering, Beijing University of Chemical Technology, Beijing 100029 China*

Received 30 November 2009; accepted 21 June 2010
DOI 10.1002/app.32999
Published online 29 September 2010 in Wiley Online Library (wileyonlinelibrary.com).

ABSTRACT: Biopolyesters poly(3-hydroxybutyrate-*co*-4-hydroxybutyrate) with an 11 mol % 4HB content [P(3HB-*co*-11%-4HB)] and a 33 mol % 4HB content [P(3HB-*co*-33%-4HB)] were blended by a solvent-casting method. The thermal properties were investigated with differential scanning calorimetry. The single glass-transition temperature of the blends revealed that the two components were miscible when the content of P(3HB-*co*-33%-4HB) was less than 30% or more than 70 wt %. The blends, however, were immiscible when the P(3HB-*co*-33%-4HB) content was between 30 and 70%. The miscibility of the blends was also confirmed by scanning electron microscopy morphology observation. In the crystallite structure study, X-ray diffraction patterns demonstrated that the crystallites of the blends were mainly from poly(3-hydroxybutyrate) units. With the addition of P(3HB-*co*-33%-4HB), larger crystallites with lower crystallization degrees were induced. Isothermal crystallization was used to analyze the melting crystallization kinetics. The Avrami exponent was kept around 2; this indicated that the crystallization mode was not affected by the blending. The equilibrium melting temperature decreased from 144 to 140°C for the 80/20 and 70/30 blends P(3HB-*co*-11%-4HB)/ P(3HB-*co*-33%-4HB). This hinted that the crystallization tendency decreased with a higher P(3HB-*co*-33%-4HB) content. © 2010 Wiley Periodicals, Inc. J Appl Polym Sci 119: 3467–3475, 2011

Key words: blends; crystallization; miscibility

INTRODUCTION

Biopolyester polyhydroxyalkanoates have attracted much attention in recent years as potential candidates for nonfossil-based thermoplastic polymers because of their thermoplasticity, biodegradability, biocompatibility, renewability, and diversified mechanical properties. Among them, poly(3-hydroxybutyrate-*co*-4-hydroxybutyrate) (P3/4HB) is a newly developed thermoplastic biopolyester synthesized by the bacterium *Ralstonia eutropha*[1] or *Alcaligenes latus*.[2] P3/4HB was originally developed to modify the rigidity of PHB materials, that is, poly(3-hydroxybutyrate) (P3HB). Depending on the different substrate feeding of 3-hydorxybutyric and 4-hydroxybutyric acid, a wide range of compositions, varying from 0 to 100 mol % 4HB unit, can be produced.[1,3–6] The composition variation leads to a wide range of mechanical properties from rigid thermoplastics to elastic rubber materials.[7] The crystallization and thermal degradation behavior of P3/4HB has been widely investigated.[8–12] The copolymers become amorphous when the 4HB content is greater than 25%.[7] These studies have also revealed that the 4HB unit acts as crystal defects in the crystallization, and with increasing 4HB content, both the crystallization degree (X_c) and the crystallization rate decrease.

Chemical modification and physical blending have both been used to improve the properties of P3/4HB materials.[13–15] Physical blending has been used frequently because of its convenience and efficiency. As an elastomer, P3/4HB possesses a low elastic modulus and fairly good tensile strength.[16] In contrast, when P3/4HB is used as a plastic, even when it has considerably good mechanical and processing properties, its crystallization is too slow, and the impact strength too poor to meet the requirements of most practical applications. In this study, amorphous and elastic P3/4HB with 33 mol % 4HB and a glass-transition temperature (T_g) of −15.75°C was blended with semicrystal P3/4HB with 11% mol 4HB [P(3HB-*co*-11%-4HB)] to investigate the miscibility and crystallization behaviors of the P3/4HB blends. We expected that the investigation would elucidate the mutual effect between the

Correspondence to: K. Xu (ktxu@stu.edu.cn) and J. He (jyhe2009@163.com).

Contract grant sponsor: National Natural Science Foundation of China; contract grant number: 20474001.
Contract grant sponsor: National High Tech 863 Grant; contract grant number: 2006AA02Z242.

semicrystallized P(3HB-*co*-11%-4HB) and the amorphous P3/4HB blend with 33 mol% 4HB [P(3HB-*co*-33%-4HB)] in the binary blends.

EXPERIMENTAL

Materials and sample preparation

P(3HB-*co*-11%-4HB) [number-average molecular weight (M_n) = 405,000 and weight-average molecular weight (M_w)/M_n = 2.15, estimated by gel permeation chromatography] and P(3HB-*co*-33%-4HB) (M_n = 538,000, M_w/M_n = 1.40, estimated by gel permeation chromatography) were provided by Tianjin Green Bioscience Materials Co., Ltd. (Tianjin, China). The 4HB molar contents in the two P3/4HB copolymers were 11 and 33%, respectively, as detected by ^{1}H-NMR. The purity of the two kinds of copolymers was also confirmed. A series of P(3HB-*co*-11%-4HB)/P(3HB-*co*-33%-4HB) blend films with different mass ratios (100/0, 90/10, 80/20, 70/30, 60/40, 50/50, 40/60, 30/70, 20/80, 10/90, and 0/100) were prepared through a conventional solvent-casting method. The blends were dissolved into chloroform at 70°C for 3 h with a total concentration of 2% (w/v). The films were cast on glass Petri dishes, and the solvent was evaporated at room temperature overnight; the resulting films were dried *in vacuo* at room temperature to completely remove the residual chloroform. They were then kept in a drying desicator at room temperature for 2 weeks to reach crystallization equilibrium before further investigation.

Differential scanning calorimetry (DSC)

Thermal properties were analyzed by a TA-Q100 DSC apparatus (TA Instruments, Texas, USA) with an autocool accessory under a nitrogen atmosphere and calibrated with indium. Samples were heated from −70 to 180°C at a heating rate (Φ) of 10°C/min. The sample was isothermally annealed at 180°C for 3 min and then rapidly quenched to −60°C at a cooling rate of 80°C/min. The quenched samples were then reheated to 180°C at the stated Φ. The T_g, melting temperature (T_m), enthalpy of fusion (ΔH_m), cold-crystallization temperature (T_{cc}; secondary or lasting crystallization temperature), and enthalpy of cold crystallization (ΔH_{cc}) were determined from the corresponding transitions in the corresponding DSC curves. The time period of cold crystallization is abbreviated as t_{max}. T_m and T_{cc} were taken as the peak value of the respective endotherm and exotherm in the DSC curve. T_g was taken as the midpoint of the specific heat increment. All results were based on the second heating run unless stated otherwise.

For the crystallization kinetic study, isothermal crystallization was used to investigate the crystallization behavior of the blends. All samples were annealed at 170°C for 3 min to destroy the thermal history. After the samples were quenched to a certain crystallization temperature (T_c), the tested temperature was maintained at T_c until the crystallization was completed. Ultimately, the temperature was quenched to −50°C again and then raised to 170°C at 20°C/min for equilibrium melting temperature (T_m^0) analysis. The exothermic crystallization peak value was recorded as a function of time t at T_c. The relative crystallinity degree of the material crystallized after time t (X_t) was calculated by means of the following equation:

$$X_t = \frac{\left(\int_0^t dH_c/dt\right)dt}{\left(\int_0^\infty dH_c/dt\right)dt} \quad (1)$$

where $\int_0^t dH_c/dt$ is the crystallization enthalpy from the initial time to time t and $\int_0^\infty dH_c/dt$ is the crystallization enthalpy from the initial time to full crystallization.

Because no melting crystallization peak could be observed from the DSC cooling scan, the nonisothermal crystallization of neat P(3HB-*co*-11%-4HB) was analyzed by cold crystallization performed through DSC at different Φ's. The samples were heated at a constant rate (selected in the range 5–40°C/min), and the exothermal curves as a function of temperature were recorded.

X-ray diffraction measurements

The X-ray diffraction spectra of the blends were recorded at 25°C on a Bruker D8 Advance diffractometer (Bruker, Karlsruhe, Germany) with nickel-filtered Cu Kα radiation (λ = 1.5406 Å; 40 KV, 40 mA) in the range 2θ = 5–50° at a scan speed of 12°/min, and the X-ray diffraction spectra were used to estimate the crystalline structure of the blends.

Scanning electron microscopy (SEM)

A JEOL JSM-6360 LA scanning electron microscope (JEOL, Tokyo, Japan) was used to study the morphology of the blend films. Surface images were recorded at a voltage of 10 kV. Before observation, the samples were coated with a thin conductive layer of gold.

RESULTS AND DISCUSSION

Miscibility of the blends

The T_g values of pure P(3HB-*co*-11%-4HB) and P(3HB-*co*-33%-4HB) were −3.8 and −15.8°C, respectively, as revealed by DSC (Table I). The blends exhibited a single T_g when the contents of P(3HB-*co*-33%-4HB) were 90, 80, 20, and 10 wt%; this demonstrated a considerable miscibility of the two

TABLE I
Thermal Properties of the P(3HB-*co*-11%-4HB)/P(3HB-*co*-11%-4HB) Blends

P(3HB-*co*-11%-4HB)/ P(3HB-*co*-33%-4HB)	T_{g1} (°C)[a]	T_{g2} (°C)[a]	T_{cc} (°C)[b]	ΔH_{cc} (J/g)[c]	T_{m1} (°C)[d]	T_{m2} (°C)[d]	ΔH_m (J/g)[e]	X_c (%)[f]
100/0	—	−3.8	53.0	29.3	113.1	126.2	33.4	25.7
90/10	—	−5.3	56.4	22.7	113.5	126.5	31.2	24.6
80/20	—	−4.9	54.8	27.6	113.1	126.7	34.3	27.8
70/30	−15.2	−5.0	57.5	25.3	114.3	127.2	22.8	18.9
60/40	−15.6	−4.3	59.8	22.8	114.5	127.7	21.1	18.0
50/50	−14.8	−5.0	59.0	22.1	114.6	127.3	19.7	17.3
40/60	−14.5	−4.9	65.6	12.4	116.7	129.6	11.2	10.1
30/70	−15.8	−4.3	65.1	10.4	117.7	118.0	7.2	6.7
20/80	−14.5	—	—	—	—	—	—	—
10/90	−15.0	—	—	—	—	—	—	—
0/100	−15.8	—	—	—	—	—	—	—

[a] T_g obtained from the second heating scan of DSC.
[b] T_{cc} determined from the second heating scan of DSC.
[c] ΔH_{cc} of the blends determined by calculation of the intensities of the exothermal peaks in the second heating scan of DSC.
[d] T_m obtained from DSC determination.
[e] Apparent ΔH_m of the blends determined by calculation of the intensities of the endothermal peaks in the second heating scan of DSC.
[f] X_c of the blends estimated from the ratio of ΔH_m of the P(3HB-*co*-11%-4HB)/P(3HB-*co*-33%-4HB) blends to that of 100% crystalline PHB (146 J/g).

copolymers in these composition ranges. To the contrary, blends with contents of P(3HB-*co*-33%-4HB) between 70 and 30 wt% displayed two T_g values with no obvious inner shift; this indicated that these two copolymer components had phase separation. The lower T_g was associated with P(3HB-*co*-33%-4HB), and the higher one corresponded to the P(3HB-*co*-11%-4HB) phase. The independence of T_g with composition implied that these two components were immiscible and, thus, gave phase separation in this composition range (Fig. 1).

The miscibility of the blends was further examined by morphological characterization. SEM observations on the surface of the blend films are shown in Figure 2. The SEM image of pure P(3HB-*co*-11%-4HB) showed a homogeneous and radiating surface, and that of pure P(3HB-*co*-33%-4HB) showed a comparatively smooth surface. Both of the pure P3/4HB film surfaces showed a close-grained texture. With increasing P(3HB-*co*-33%-4HB) content, the blend films revealed more cavities on the surface. Typically, an isolated island structure appeared at a 50 wt% P(3HB-*co*-33%-4HB) content. When the amount of P(3HB-*co*-33%-4HB) exceeded 50 wt%, phase inversion occurred. The radiating structure appeared again and showed homogeneity.

Thermal behaviors

Melting behaviors and crystalline structure of the blends

The multiple melting phenomena of most semicrystalline polymers has been observed and investigated extensively for decades.[17,18] P(3HB-*co*-11%-4HB) is a typical semicrystalline copolymer. With the exception of pure P(3HB-*co*-33%-4HB) and P(3HB-*co*-33%-4HB) with weight ratios of 80 and 90 wt% in the blends, which showed no melting peak, the remaining blends, including pure P(3HB-*co*-11%-4HB), possessed double melting peaks (Fig. 1). This phenomenon was interpreted from the model of the melting, recrystallization, and remelting processes.[19] T_{m1} is the melting temperature of the original or primary crystals formed, and T_{m2} is the melting temperature of the recrystallized crystallites from the original crystals. With increasing P(3HB-*co*-33%-4HB) content, both T_{m1} and T_{m2} increased (Table I); T_{cc} also increased.

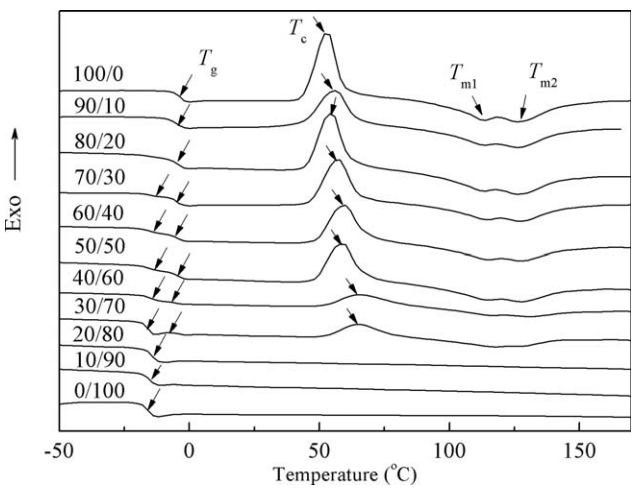

Figure 1 DSC thermograms of the P(3HB-*co*-11%-4HB)/P(3HB-*co*-33%-4HB) blends from the second heating run (5°C/min).

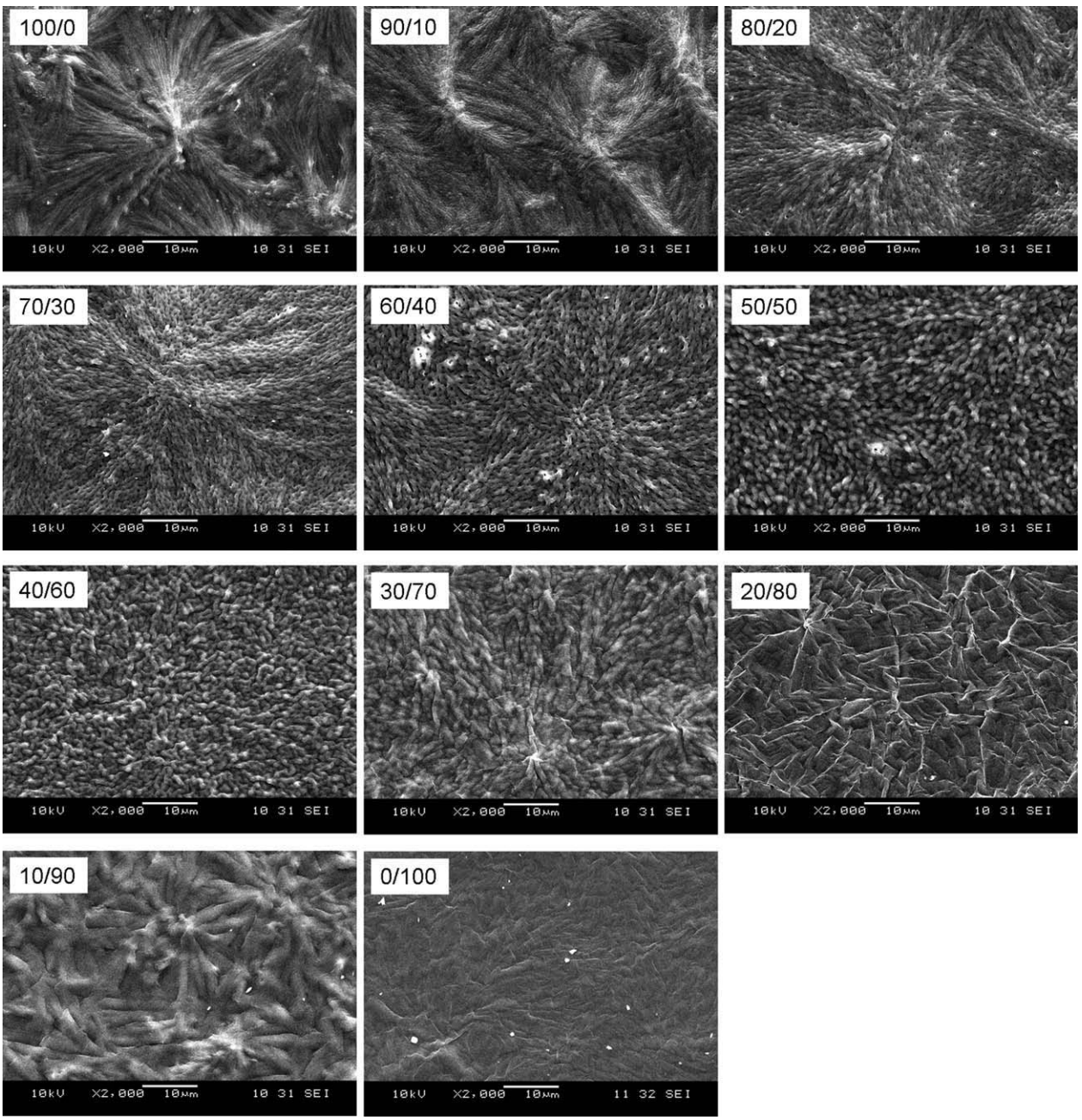

Figure 2 Morphological observation of the P(3HB-*co*-11%-4HB)/P(3HB-*co*-33%-4HB) blends by SEM.

The increase in T_m means that the better crystal formed. This hinted that the lower T_g P(3HB-*co*-33%-4HB) portion functioned as plasticizer to increase the chain mobility of P(3HB-*co*-11%-4HB) to arrange into better crystals, as the chain mobility would have been of benefit to polymer chain rearrangement in the crystal lattice. However, the increase in T_{cc} would have, thus, revealed the lower crystallization tendency of the blends. With increasing P(3HB-*co*-33%-4HB) content, X_c also decreased. This might have been induced from lower crystal nucleation as P(3HB-*co*-33%-4HB) also acted as diluent for the crystallizable P(3HB-*co*-11%-4HB), which reduced the nucleation number and, thus, the rate of the crystallization process.[20] This also caused a decrease in X_c of P(3HB-*co*-11%-4HB) (Table I). Herein, X_c is defined as the ratio of the melting enthalpy (ΔH_m) to that of 100% crystalline P3HB (146 J/g)[21] and calculated from the following equation:

$$X_c(\%) = 100 \times \Delta H_m / \Delta H_f \times W_{\mathrm{P3HB}} \qquad (2)$$

where $\Delta H_f = 146$ J/g and W_{P3HB} is the P3HB fraction in the blends.

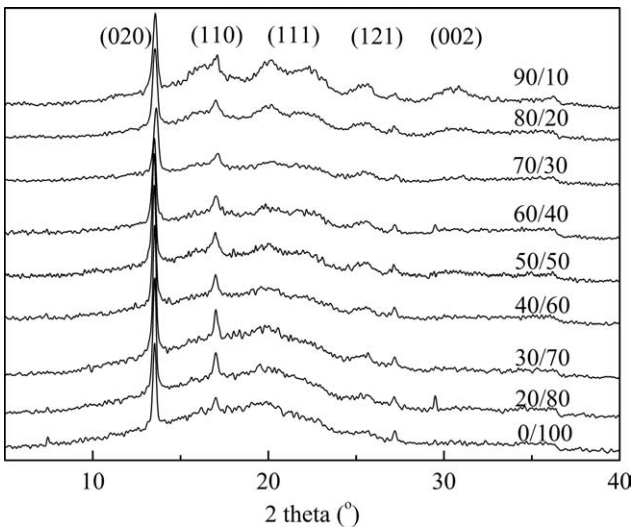

Figure 3 X-ray diffraction profile of the P(3HB-*co*-11%-4HB)/P(3HB-*co*-33%-4HB) blends.

The crystalline structures of the blends were investigated by X-ray diffraction (Fig. 3). The crystalline structures of P3/4HB were P3HB lattices,[8] and the diffraction peaks of the crystals appeared around 13.5, 17.1, 22.4, 25.6, and 30.7°; these peaks corresponded to the (020), (110), (111), (121), and (002) crystallographic planes, respectively.[22] It was clear that the *d*-spacing values (Table II) were almost different invariant for the (020), (110), and (002) crystallographic planes, which indicated that the parameters of the P3HB unit cell did not change in these blend systems. The P3HB crystal lattice was still observed from the blends when the content of P(3HB-*co*-33%-4HB) was up to 50 wt %. In addition, the diffraction peaks of the (020) and (110) planes became higher and more narrow with increasing P(3HB-*co*-33%-4HB) content. This was consistent with the DSC results, as better crystals were formed. The calculated crystallite sizes in the (020) direction are listed in Table II. The P(3HB-*co*-11%-4HB) crystallites were clearly enlarged in this direction. This result confirmed that the larger crystal formed because the addition of P(3HB-*co*-33%-4HB) provided a less crystal nucleus and, thus, larger crystallites, as discussed previously. Because of the two different kinds of testing mechanisms, the crystallinity obtained by X-ray diffraction was generally higher than that obtained by DSC. Usually, we used the crystallinity data from DSC to define X_c of the polymers.

TABLE II
Degree of Crystallinity and *d*-Spacing of the P(3HB-*co*-11%-4HB)/P(3HB-*co*-33%-4HB) Blends Determined from X-Ray Diffraction

P(3HB-*co*-11%-4HB)/ P(3HB-*co*-33%-4HB)	L_{020} (Å)	*d*-spacing (nm)		
		(020)	(110)	(002)
90/10	269	0.652	0.519	0.294
80/20	279	0.652	0.521	0.291
70/30	279	0.649	0.516	0.289
60/40	295	0.654	0.520	0.290
50/50	296	0.655	0.521	0.292
40/60	312	0.654	0.522	—
30/70	309	0.654	0.521	—
20/80	327	0.654	0.521	—
0/100	334	0.654	0.521	—

Nonisothermal cold-crystallization behavior of neat P(3HB-co-11%-4HB)

The crystallization exothermal curves of P(3HB-*co*-11%-4HB) at different Φ's are given in Figure 4. The peak value for maximum cold crystallization (T_{cc})

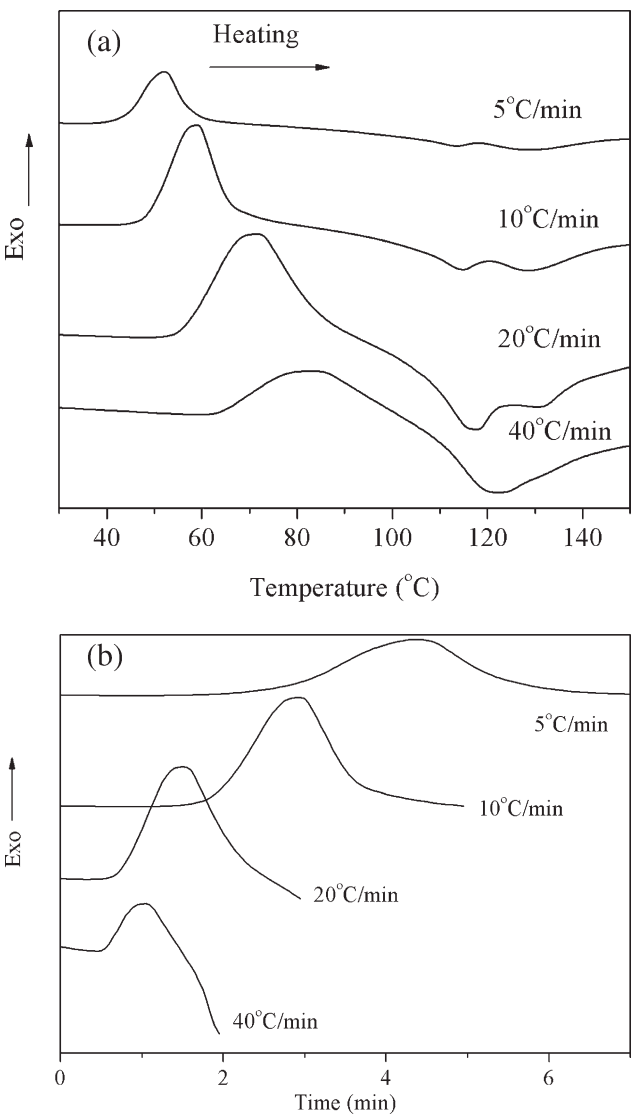

Figure 4 DSC thermograms of the nonisothermal cold crystallization for neat P(3HB-*co*-11%-4HB) at different Φ's (a) versus temperature and (b) versus time.

TABLE III
Nonisothermal Cold Crystallization of Neat P(3HB-*co*-11%-4HB)

Φ (°C/min)	T_{cc} (°C)[a]	t_{max} (min)[b]	ΔH_{cc} (J/g)[c]
5	52.0	6.32	26.32
10	59.0	4.17	31.75
20	71.4	2.24	26.00
40	83.5	1.05	6.58

[a] Peak temperature for maximum crystallization at different Φ's obtained from the second heating scan of DSC.
[b] Corresponding t_{max} of nonisothermal cold crystallization at different Φ's obtained from the second heating scan of DSC.
[c] Crystallization enthalpy at different Φ's determined from the second heating scan of DSC.

shifted to a high temperature when Φ was increased. The corresponding t_{max}, or peak width, also became shorter with increasing Φ [Fig. 4(b), Table III]. This was interpreted from the nucleation mechanism and crystal growth geometries for the primary and secondary crystallization processes.[23,24] When the sample had a lower Φ, there was enough time for the molecular chain to form the necessary nuclei and then arrange into a better crystallite. The longer time enhanced the mobility of the polymer chain and made the cold crystallization happen at a lower temperature and in a narrower temperature range. As Φ increased, the polymer chains experienced a shorter time. In this case, they needed a higher mobility to compact into crystallites at this shorter time, and thus, T_{cc} happened at a higher temperature. A shorter t_{max} and a higher T_{cc} were observed [Fig. 4(a,b)]. Meanwhile, at a higher Φ, the polymer chain had no time to form a better nucleus and arranged into only poor crystallites. The relaxation of the polymer chains did not follow the change in the temperature. Thus, a broader cold-crystallization exothermal peak was encountered. The following one broad melting peak hinted that the recrystallization of the primary crystals did not happen at higher Φ [Fig. 4(a)].

Isothermal crystallization kinetics of the blends

An isothermal crystallization study of the P(3HB-*co*-11%-4HB)/P(3HB-*co*-33%-4HB) blends was carried out with a cooling rate of 5°C/min (Fig. 5) to a constant temperature. At even this slow cooling rate, the melting crystallization peak of neat P(3HB-*co*-11%-4HB) was still not observed, possibly because of the too-slow crystallization rate of the P3/4HB materials. However, it gave optimal melting crystallization peaks of the 80/20 and 70/30 P(3HB-*co*-11%-4HB)/P(3HB-*co*-33%-4HB) blends. As we know, P(3HB-*co*-33%-4HB) is amorphous and flexible elastomer, and the flexibility of the polymer chain is favorable to the polymer crystallization process. On the other hand, when the chain flexibility and the amorphous region in blends are increased profoundly, the crystallization domain is damaged by the amorphous domain and X_c becomes low. In our study, when the amount of P(3HB-*co*-33%-4HB) exceeded 40 wt %, the blends showed a lack of crystallization ability.

To investigate further, isothermal melting crystallization was used to study the melting crystallization properties and evaluate the crystallization kinetics for the 80/20 and 70/30 blends. The overall isothermal crystallization kinetics of the blends were analyzed on the basis of the well-known Avrami equation. We assumed that X_t developed as a function of crystallization time t, as follows:

$$1 - X_t = \exp(-kt^n) \tag{3}$$

$$\lg[-\ln(1 - X_t)] = \lg k + n \lg t \tag{4}$$

where n is the Avrami exponent, which depends on the nature of nucleation and the growth geometry of the crystals, and k is the crystallization rate constant, which depends on nucleation and the crystal growth rate.[25,26] The guidelines suggested by Müller et al.[27] were used to prevent common problems on the use of the Avrami equation to fit the data. In Avrami analysis, the ratio of the area at time t to the area of the whole exotherm was used to get X_t. Figure 6 shows the development of X_t as a function of the crystallization time t for both the 80/20 and 70/30 P(3HB-*co*-11%-4HB)/P(3HB-*co*-33%-4HB) blends. The crystallization time presented a typical Avrami curve with increasing T_c for both the 80/20 and 70/30 blends.

From the slope and intercept values of the curves, n and k were obtained (Fig. 7). The crystallization parameters n and k are listed in Table IV. There was no significant change in n, which was around 2 in

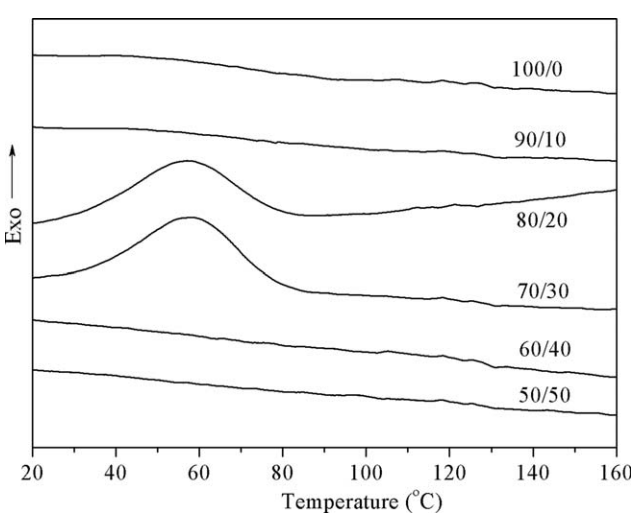

Figure 5 Melting crystallization of the P(3HB-*co*-11%-4HB)/P(3HB-*co*-33%-4HB) blends as determined by DSC (cooling rate = 5°C/min).

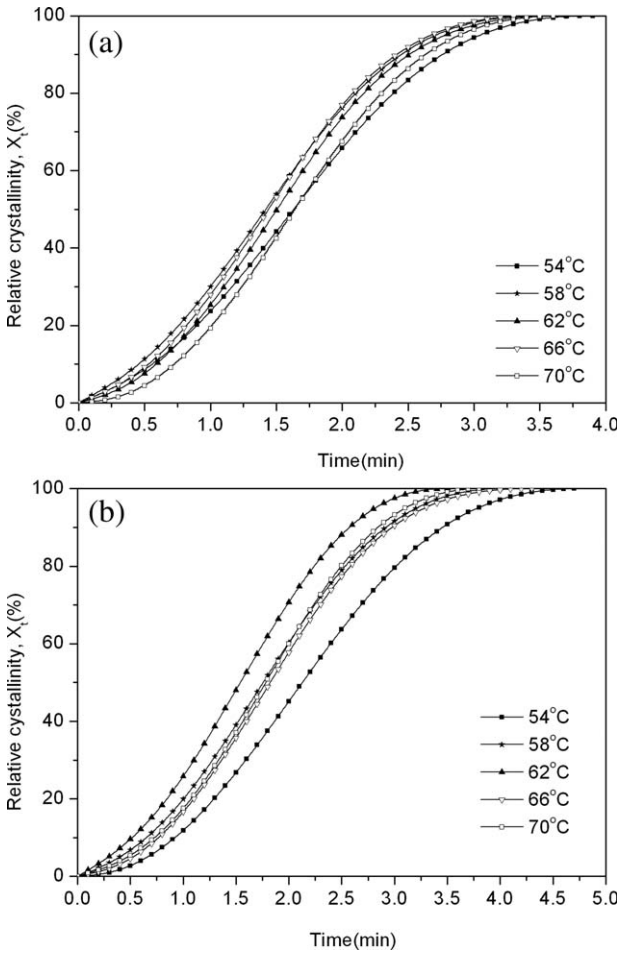

Figure 6 X_t versus the crystallization time for the P(3HB-*co*-11%-4HB)/P(3HB-*co*-33%-4HB) [(a) 80/20 and (b) 70/30] blend films at different T_c values.

the two blends. This indicated that in the T_c range of isothermal experiments, both the nucleation mechanism and geometry of crystal growth of the blends were almost not affected by the composition and T_c. In general, $n = 2$ corresponds to two distinct kinds of possible crystallization mechanisms. One is two-dimensional crystal growth under heterogeneous nucleation; the other is one-dimensional crystal growth under homogeneous nucleation. No clear spherulitic morphology was observed in the polarizing optical microscopy (POM) observation of these two blends (graphs are not given). The melting crystallization behavior study showed that the thermal motion of the P(3HB-*co*-33%-4HB) chain improved the crystallization ability in the blends. As we know, homogeneous nucleation is caused by the thermal motion of the molecular chain. Thus, we inferred that the blends (80/20 and 70/30) were homogeneous nucleation systems and formed needlelike crystals.

Furthermore, when T_c was increased in the temperature range 54–70°C, the parameter k reached a maximum value at certain temperature, which in the 80/20 blend was at 58°C and in the 70/30 blend was at 62°C. The overall crystallization rate (k) of the 70/30 blend was somewhat lower than that of the 80/20 blend at the same T_c, and the maximum value k shifted to a higher temperature. This was possibly due to the lower nucleation ability. Usually, a higher temperature is favorable for the crystal growth rate and inhibitory to nucleation. In the T_c range, nucleation and crystal growth are competitive factors.[28] This is also related to the homogeneous nucleation mechanism.

Meanwhile, the half-life crystallization time ($t_{0.5}$), which is defined as the time at $X_t = 50\%$, is an important parameter for the crystallization kinetics; it can also be calculated with the following relation:

$$t_{0.5} = \left(\frac{\ln 2}{k}\right)^{1/n} \tag{5}$$

As shown in Table IV, clearly, $t_{0.5}$ for 80/20 was shorter than that for 70/30. According to the foregoing analysis on crystallization kinetics, we

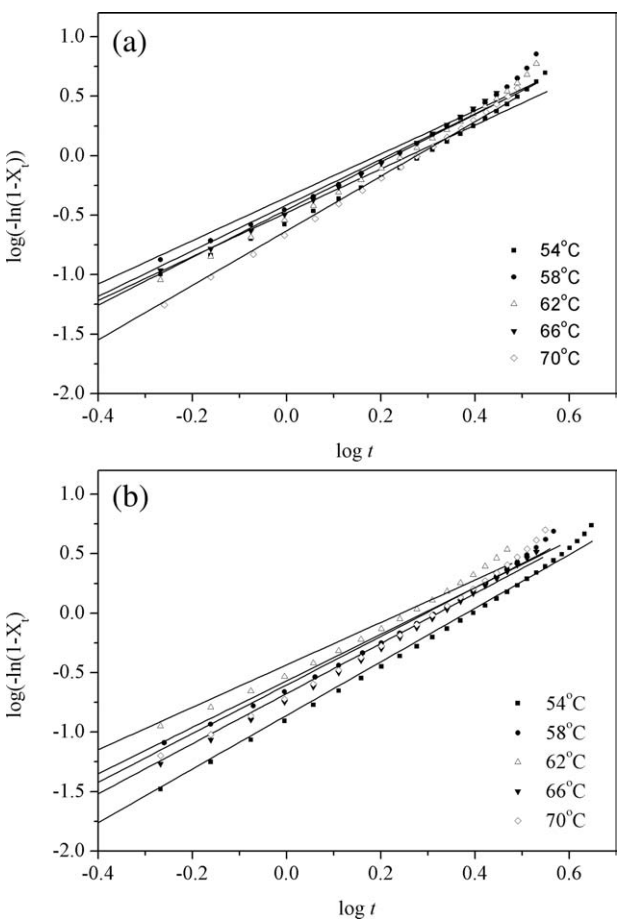

Figure 7 Avrami plots of the P(3HB-*co*-11%-4HB)/P(3HB-*co*-33%-4HB) blends [(a) 80/20 and (b) 70/30] at different T_c values.

concluded that the 80/20 composition exhibited the better crystallization ability in the P(3HB-*co*-11%-4HB)/P(3HB-*co*-33%-4HB) blend system. Furthermore, for the 80/20 blend, the value of $t_{0.5}$ almost did not change with increasing melting T_c, which indicated that the change in T_c had little effect on $t_{0.5}$. However, for the 70/30 blend, $t_{0.5}$ maintained a decreasing trend with temperature.

Figure 8 shows the linear relationship between T_m and melting T_c in the isothermal crystallization study for both blends. T_m^0 was determined by extrapolation to the lines of $T_m = T_c$ according to the Hoffman–Weeks equation:

$$T_m = \left(1 - \frac{1}{\beta}\right) T_m^0 + \frac{1}{\beta} T_c \quad (6)$$

where β is the ratio of the initial lamellar thickness to the final lamellar thickness and the value of $1/\beta$ was between 0 ($T_m = T_m^0$ for all T_c's in the case of most stable crystals) and 1 ($T_m = T_c$ in the case of inherently unstable crystals).[29,30] The values of $1/\beta$ obtained from the slopes were 0.349 and 0.318 for the 80/20 and 70/30 P(3HB-*co*-11%-4HB)/P(3HB-*co*-33%-4HB) blends, respectively. This showed that the crystal in the 70/30 blend was more stable than that of 80/20 blend. T_m^0 was obtained from the intersection of the line T_m, which was a function of T_c for the blends, and the line $T_m = T_c$. Actually, there existed two melting peaks after isothermal crystallization (data not shown). The higher melting peak was ascribed to the melting process of the recrystallized crystallites, whereas the lower melting peak corresponded to the melting of the original or primary crystals existing before the DSC scan.[31] The lower T_m was chosen to calculate the T_m^0 values according to the previous research.[32] The values of T_m^0 for the 80/20 and 70/30 P(3HB-*co*-11%-4HB)/P(3HB-*co*-33%-4HB) blends were 144 and 140°C, respectively. This meant that the value of T_m^0 decreased with increasing P(3HB-*co*-33%-4HB). Generally, *undercooling* is defined as $T_m^0 - T_c$, which is considered as the thermodynamic driving force for the crystal growth process.[26] The lower the value of $T_m^0 - T_c$ is, the slower the crystal growth rate was. This was the explanation for why the crystallization rate k became lower whereas increasing content of P(3HB-*co*-33%-4HB) at the 80/20 and 70/30 blends.

TABLE IV
Isothermal Melting Crystallization Kinetics Parameters of the P(3HB-*co*-11%-4HB)/P(3HB-*co*-33%-4HB) Blends

P(3HB-*co*-11%-4HB)/ P(3HB-*co*-33%-4HB)	T_c (°C)	k	n	$t_{0.5}$ (min)
80/20	54	3.311×10^{-1}	1.8	1.485
	58	4.467×10^{-1}	1.8	1.268
	62	3.548×10^{-1}	2.0	1.393
	66	3.846×10^{-1}	1.9	1.361
	70	2.339×10^{-1}	2.3	1.622
70/30	54	1.380×10^{-1}	2.3	4.056
	58	2.691×10^{-1}	2.0	5.482
	62	3.715×10^{-1}	1.8	2.080
	66	2.109×10^{-1}	2.1	1.771
	70	1.836×10^{-1}	2.0	1.758

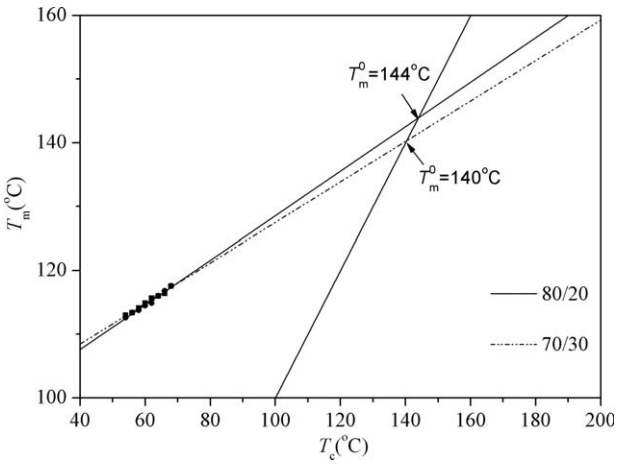

Figure 8 Hoffman–Weeks plots of the P(3HB-*co*-11%-4HB)/P(3HB-*co*-33%-4HB) (70/30) and (80/20) blends for the estimation of T_m^0.

CONCLUSIONS

Blend miscibility through DSC study revealed that P(3HB-*co*-11%-4HB) was miscible with P(3HB-*co*-33%-4HB) when the later content was less than 30% or more than 70%. Immiscibility was observed at P(3HB-*co*-33%-4HB) contents between 30 and 70%. The crystalline structure in the blends was mainly from P3HB and was not affected by the blend composition. The isothermal crystallization was analyzed via the Avrami equation. n was kept at 2, and the crystallization mode was not affected by the blends. k changed with the composition of the blends. With the addition of P(3HB-*co*-33%-4HB), the crystallization of P(3HB-*co*-11%-4HB) was enhanced. However, more P(3HB-*co*-33%-4HB) decreased the crystallization. This was also confirmed by T_m^0 analysis. Interestingly, the 80/20 P(3HB-*co*-11%-4HB)/P(3HB-*co*-33%-4HB) gave a crystallization rate with no dependence on temperature.

References

1. Ishida, K.; Wang, Y.; Inoue, Y. Biomacromolecules 2001, 2, 1285.
2. Nakamura, S.; Doi, Y.; Scandola, M. Macromolecules 1992, 25, 4237.
3. Hori, Y.; Yamaguchi, A.; Hagiwara, T. Polymer 1995, 36, 4703.
4. Doi, Y.; Segawa, A.; Kunioka, M. Int J Biol Macromolecules 1990, 12, 106.

5. Shi, F.; Ashby, R. D.; Gross, R. A. Macromolecules 1997, 30, 2521.
6. Kimura, H.; Ohura, T.; Takeishi, M.; Nakamura, S.; Doi, Y. Polym Int 1990, 48, 1073.
7. Doi, Y. Microbial Polyesters; VCH: New York, 1990.
8. Kunioka, M.; Tamaki, A.; Doi, Y. Macromolecules 1989, 22, 694.
9. Mitomo, H.; Doi, Y. Int J Biol Macromol 1999, 25, 201.
10. Kunioka, M.; Doi, Y. Macromolecules 1990, 23, 1933.
11. Yoon, J. S.; Chin, I. J.; Kim, M. N.; Kim, C. Macromolecules 1996, 29, 3303.
12. Doi, Y.; Kanesawa, Y.; Kunioka, M.; Saito, T. Macromolecules 1990, 23, 26.
13. Pan, J. Y.; Li, G. Y.; Chen, Z. F.; Chen, X. Y.; Zhu, W. F.; Xu, K. T. Biomaterials 2009, 30, 2975.
14. Zhu, W. F.; Wang, X. J.; Chen, X. Y.; Xu, K. T. J Appl Polym Sci 2009, 114, 3923.
15. Wang, X. J.; Chen, Z. F.; Chen, X. Y.; Pan, J. Y.; Xu, K. T. J Appl Polym Sci 2010, 117, 838.
16. Avella, M.; Martuscelli, E.; Raimo, M. J Mater Sci 2000, 35, 523.
17. Woo, E. M.; Ko, T. Y. Colloid Polym Sci 1996, 274, 309.
18. Yeh, J. T.; Runt, J. J Polym Sci Part B: Polym Phys 1989, 27, 1543.
19. Ju, M. Y.; Chang, F. C. Polymer 2001, 42, 5037.
20. Ni, C. Y.; Luo, R. C.; Xu, K. T.; Chen, G. Q. J Appl Polym Sci 2009, 111, 1720.
21. Barham, P. J.; Keller, A.; Otum, E. L.; Holmes, P. A. J Mater Sci 1984, 19, 2781.
22. Fei, B.; Chen, C.; Wu, H.; Peng, S. W.; Wang, X. Y.; Dong, L. S.; Xin, J. H. Polymer 2004, 45, 6275.
23. Chen, Q. Y.; Yu, Y. N.; Na, T. H.; Zhang, H. F.; Mo, Z. J Appl Polym Sci 2002, 83, 2528.
24. Liu, T.; Mo, Z. S.; Wang, S. E.; Zhang, H. F. Polym Eng Sci 1997, 37, 568.
25. Avrami, M. J Chem Phys 1939, 7, 1103.
26. Avrami, M. J Chem Phys 1940, 8, 212.
27. Lorenzo, A. T.; Arnal, M. L.; Albuerne, J.; Müller, A. J. Polym Test 2007, 26, 222.
28. Wunderlich, B. Macromolecular Physics; Academic: New York, 1973.
29. Zhang, L. L.; Goh, S. H.; Lee, S. Y.; Hee, G. R. Polymer 2000, 41, 1429.
30. Hoffman, J. D.; Weeks, J. J. J Res Natl Bur Stand Sect A 1962, 66, 13.
31. Qiu, Z. B.; Ikehara, T.; Nishi, T. Polymer 2003, 44, 3095.
32. Liu, W. J.; Yang, H. L.; Wang, Z.; Dong, L. S.; Liu, J. J. J Appl Polym Sci 2002, 86, 2145.